Microfluidic "jets" for generating steady-state gradients of soluble molecules on open surfaces

Thomas M. Keenan
Department of Bioengineering, University of Washington, Seattle, Washington 98195

Chia-Hsien Hsu
Department of Mechanical Engineering, University of Washington, Seattle, Washington 98195

Albert Folch[a)]
Department of Bioengineering, University of Washington, Seattle, Washington 98195

(Received 8 April 2006; accepted 25 July 2006; published online 12 September 2006)

The ability to control the spatiotemporal microenvironment of cultured cells, such as cells in soluble gradients of signaling molecules, is critical for understanding the quantitative relationship between physicochemical signals and the induced biological responses. Existing methods for generating biomolecule gradients either offer little control, result in poor reproducibility, and/or place cells in potentially confounding or adverse conditions. Here the authors report the generation of soluble gradients by a system of microfluidic "jets" that inject picoliter amounts of fluid into an open pool with negligible exposure of the surface to flow. A stable, reproducible gradient can be formed in minutes. © *2006 American Institute of Physics*. [DOI: 10.1063/1.2345914]

Gradients of diffusible signaling molecules play essential roles in many biological phenomena including development, cancer, inflammation, and wound healing. Cells have been exposed to diffusible gradients in cultures using biological gels (e.g., collagen,[1] fibrin,[2] or agarose[3]), glass micropipettes,[4] and a variety of static-chamber devices (e.g., the chambers of Boyden,[5] Zigmond,[6] and Zicha *et al.*[7]). Although instrumental in furthering many biological studies, all of these methods generate gradients that change with time and position and are difficult to control and characterize quantitatively. A laminar-flow, microfluidic gradient generator developed by Dertinger *et al.*[8] can generate steady-state gradients that are quantifiable and user controlled, but with several limitations. (1) The device can only generate gradients under fluid flow, which induces shear and drag forces that may alter intracellular signaling[9–12] or cause changes in cell shape and attachment that may lead to migrational bias.[13] (2) The gradient evolves as the fluid flows downstream such that cells in the microchannel do not all experience the same concentration gradient. (3) Downstream cells are exposed to higher concentrations of cell-secreted molecules (e.g., metabolites and growth factors) than upstream cells, which precludes true redundancy in single-cell data. (4) The observation area is an enclosed microfluidic channel, which limits gas and nutrient exchange for long term cell viability and hinders physical access to single cells (e.g., patch-clamp recording, intracellular injection, atomic force microscopy, etc.) during the course of the experiment.

Here we present a microfluidic device that generates gradients of diffusible molecules in an open reservoir without the complications associated with closed-microchannel environments or with fluid flow. The fabrication and principle of operation of the device are shown schematically in Fig. 1. The device is fabricated in poly(dimethyl)siloxane (PDMS) using a soft-lithographic method for contact-transferring PDMS microstructures.[14] Briefly, the features of a three-level mold [Fig. 1(a)] are defined by one electron-beam lithography step (features 1.5 μm in height) followed by two photolithography steps (one for 45-μm-high features and one for 66-μm-high features). PDMS is applied and excluded from the tallest features of the three-level mold by compressing the mold against a polyester sheet [Fig. 1(b)]. After the PDMS cures [Fig. 1(c)], the sheet is peeled away from the mold [Fig. 1(d)]. The PDMS structures are released with the sheet and can be transferred to a glass substrate by oxygen plasma bonding[14] [Fig. 1(e)]. The resulting device contains an open reservoir 66 μm deep and 200 μm wide. Two 45-μm-tall and 100-μm-wide microchannels serve as manifolds to deliver fluids to each array of 25-μm-long channels (1.5×1.5 μm^2 cross section). Pressurization of the mani-

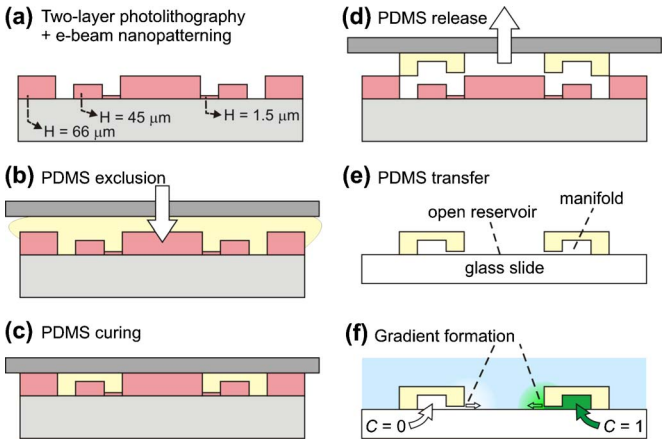

FIG. 1. (Color online) (a) Electron-beam lithography and two-layer photolithography using SU-8 photoresist are used to fabricate a three-level mold. (b) PDMS is applied and excluded from the tallest features by compressing a plastic sheet against the mold. (c) The PDMS is thermally cured and (d) peeled from the mold using the plastic sheet as a flexible support. (e) The PDMS structures are bonded to a glass slide using oxygen plasma treatment. (f) Manifolds are filled with either diluent ($C=0$) or a solution of the diffusing molecule ($C=1$) and pressurized to cause the fluid in the manifold to be ejected into the open reservoir via the μFJ.

[a)]Author to whom correspondence should be addressed; electronic mail: afolch@u.washington.edu

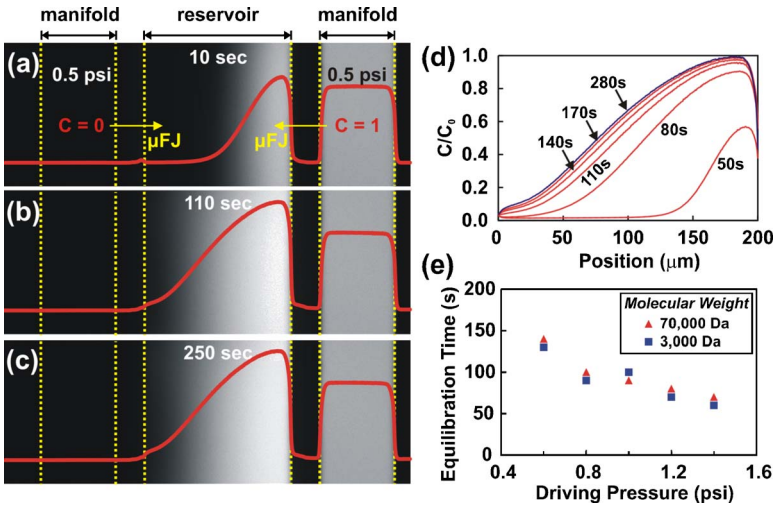

FIG. 2. (Color online) [(a)–(c)] Top-view confocal fluorescence micrographs of the device (10 μm optical slice nearest the surface) in operation taken at (a) 10 s, (b) 110 s, and (c) 250 s; the left and right manifolds are loaded with water and fluorescent dextran (70 kDa), respectively, and pressurized at $P_L=P_R=0.5$ psi. The reservoir is 200 μm wide. Overlaid are the fluorescence intensity image-wide line scans (solid curves) representing the average dextran concentration profile near the surface of the reservoir and manifolds. Note that within a few minutes the gradient becomes indistinguishable from later time points. (d) Relative dextran concentration (C/C_0) profile for various time points, showing that the gradient approaches steady state asymptotically with time. (e) Plot of the equilibration time vs applied pressure. The gradient equilibrates faster as the pressure increases, with no detectable dependence on molecular weight in the 3–70 kDa range.

folds causes fluid to be ejected (~40–150 pl/min) at the μFJ locations [Fig. 1(f)], effectively "pinning" the μFJ outlet concentration to that inside the manifold. A stable gradient can be established within minutes.

Gradient formation at the surface of the open reservoir can be quantified by acquiring time-lapse confocal fluorescence micrographs (10-μm-thick optical slices, 10 s interval) and using solutions of fluorescently labeled dextrans as models of biological molecules. Either Oregon green-labeled dextran (70 kDa) or Cascade blue-labeled dextran (3 kDa) is loaded into one of the manifolds and the diluent (water) is loaded into the other manifold prior to pressurization ($P\sim0.4-1.6$ psi) with nitrogen gas. Shown in Figs. 2(a)–2(c) are example confocal micrographs of 70 kDa dextran gradients ($P=0.5$ psi) overlaid with the corresponding image-wide line scans (i.e., concentration profiles). Fluorescence intensity is within the detection limits of the (highly linear) charge-coupled device detector and thus proportional to the dextran concentration. A concentration gradient is quickly established [Fig. 1(a)] and rapidly (within ~2 min) becomes indistinguishable [Fig. 2(b)] from much later time points [Fig. 2(c)]. With time, the concentration profile asymptotically approaches steady state (as defined by a <5% variation of all the line scan values over 10 s) [Fig. 2(d)], unlike flow-based or chamber-based gradient generators where irreproducible flow patterns can occur during gradient formation. All gradients generated with the μFJ device reach steady state in <4 min for driving pressures ≥0.5 psi. For the range of molecular weights (3–70 kDa) that were tested in this study, the equilibration time is virtually independent of the molecular weight [Fig. 2(e)].

A salient feature of our device is that it allows for dynamically adjusting the slope and position of the gradient independently (Fig. 3). Figures 3(a)–3(c) show confocal images of 70 kDa dextran gradients overlaid with the corresponding concentration profiles for three combinations of left and right manifold pressures (P_L and P_R, respectively). Figure 3(d) [and comparison of Figs. 3(a) and 3(b)] demonstrates that equal increases in pressure ($\Delta P=0$, 0.4, and 0.7 psi) delivered to each manifold narrow the linear gradient region and increase the peak magnitude of the gradient without causing an obvious change in the peak position. In contrast, Fig. 3(e) [and comparison of Figs. 3(b) and 3(c)] shows that when the left manifold pressure (P_L) is increased and the right manifold pressure (P_R) is decreased by the same magnitude (here, increments/decrements of 0.4 and 0.8 psi), the gradient shape is virtually unchanged while the gradient position shifts to the right (shifts of ~8 and ~12.5 μm, respectively).

The mass and momentum transport within the device can be understood by finite element modeling (FEMLAB 3.1, Comsol Inc., Burlington, MA) of an infinite slit. (The infinite slit has ~50 times less fluid resistance than the actual array of μFJ, so the model driving pressures P_{mod} have to be reduced by the same factor with respect to the experimental driving pressures P_{expt}; the 50× factor is estimated by matching the

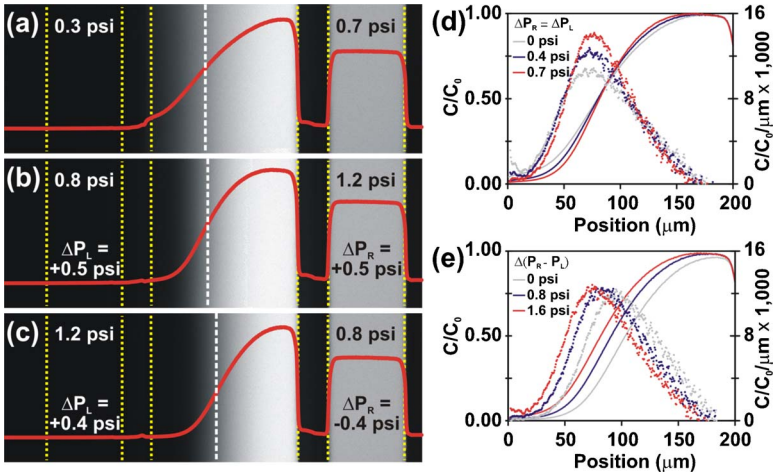

FIG. 3. (Color online) [(a)–(c)] Top-view confocal fluorescence micrographs and the corresponding steady-state 70-kDa dextran surface concentration profiles (solid curves) at the indicated P_L and P_R. The reservoir is 200 μm wide. The dashed white vertical line indicates the position of maximum slope (gradient). (d) Relative dextran (70 kDa) concentration profiles (C/C_0, solid lines) and the corresponding gradients (derivative of C/C_0, dots) before and after equal increases in P_L and P_R. The gradient increases in magnitude but does not shift as both pressures increase equally. (e) Concentration profiles (solid lines) and the corresponding gradients (dots) before and after P_R and P_L are increased and decreased, respectively, by the same amount. The gradient shifts towards the left but does not change in magnitude.

shapes of the experimental gradients with those of the modeled gradients, as shown in Ref. 15.) The model provides indirect knowledge of the fluid velocity generated by the μFJ, revealing that the flow lines are directed upwards (Ref. 15). The horizontal component of the fluid velocity in the 10 μm immediately above the open reservoir surface is greatest at the μFJ outlets and, due to isotropic transfer of momentum, rapidly decreases with distance from the outlets (V_{sx}=250–835 μm/s at x=0 and V_{sx}=22–75 μm/s at x=10 μm for P_{expt} ranging 0.5–1.5 psi; see Ref. 15). In comparison, the microfluidic gradient generator by Dertinger *et al.*,[8] Walker *et al.*,[13] and Jeon *et al.*[16] operating at common flow rates of 1–3 μl/min generates fluid velocities in the 10 μm nearest the surface of ~500–1500 μm/s and shear stresses that can introduce chemotactic migration bias (~0.7 dyn/cm^2).[13] Our model predicts that less than 5% of the reservoir surface is exposed to shear stresses >0.7 dyn/cm^2 (Ref. 15), indicating that the distance from the wall below which cell migration might be biased by external forces is on the order of only a few microns (Ref. 15, inset).

In summary, we believe that μFJ is a powerful tool for generating reproducible gradients of diffusible molecules for applications where fluid flow, shear forces, and closed volumes are known or suspected to have adverse effects on cells, and where 4 min gradient stabilization times are acceptable. Although in this demonstration we used μFJ arrays to create a one-dimensional gradient, more complex gradient topologies can be generated through different μFJ arrangements, opening the way for studies of cells responding to multiple signaling molecules.

[1] A. F. Brown, J. Cell. Sci. **58**, 455 (1982).
[2] P. C. Wilkinson and J. M. Lackie, Exp. Cell Res. **145**, 255 (1983).
[3] R. D. Nelson, P. G. Quie, and R. L. Simmons, J. Immunol. **115**, 1650 (1975).
[4] R. W. Gundersen and J. N. Barrett, J. Cell Biol. **87**, 546 (1980).
[5] S. Boyden, J. Exp. Med. **115**, 453 (1962).
[6] S. H. Zigmond, J. Cell Biol. **75**, 606 (1977).
[7] D. Zicha, G. A. Dunn, and A. F. Brown, J. Cell. Sci. **99**, 769 (1991).
[8] S. K. W. Dertinger, D. T. Chiu, N. L. Jeon, and G. M. Whitesides, Anal. Chem. **73**, 1240 (2001).
[9] B. D. Matthews, D. R. Overby, R. Mannix, and D. E. Ingber, J. Cell. Sci. **119**, 508 (2006).
[10] Y. Komai and G. W. Schmid-Schonbein, Ann. Biomed. Eng. **33**, 1375 (2005).
[11] E. Hentzen, D. McDonough, L. McIntire, C. W. Smith, H. L. Goldsmith, and S. I. Simon, Ann. Biomed. Eng. **30**, 987 (2002).
[12] M. Okuyama, Y. Ohta, J. Kambayashi, and M. Monden, J. Cell. Biochem. **63**, 432 (1996).
[13] G. M. Walker, J. Q. Sai, A. Richmond, M. Stremler, C. Y. Chung, and J. P. Wikswo, Lab Chip **5**, 611 (2005).
[14] C.-H. Hsu, C. Chen, and A. Folch, Lab Chip **5**, 420 (2004).
[15] See EPAPS Document No. E-APPLAB-89-272636 for supplementary Fig. S1. This document can be reached via a direct link in the online article's HTML reference section or via the EPAPS homepage (http://www.aip.org/pubservs/epaps.html).
[16] N. L. Jeon, H. Baskaran, S. K. W. Dertinger, G. M. Whitesides, L. Van de Water, and M. Toner, Nat. Biotechnol. **20**, 826 (2002).